THE ASTROPHYSICAL JOURNAL, 482:929–941, 1997 June 20

BINARY-INDUCED NEUTRON STAR COMPRESSION, HEATING, AND COLLAPSE

G. J. MATHEWS
University of Notre Dame, Department of Physics, Notre Dame, IN 46556

AND

J. R. WILSON
University of Notre Dame, Department of Physics, Notre Dame, IN 46556 and University of California, Lawrence Livermore National Laboratory, Livermore, CA 94550

Received 1996 June 10; accepted 1997 January 7

ABSTRACT

We analyze several aspects of the recently noted neutron star collapse instability in close binary systems. We utilize (3 + 1) dimensional and spherical numerical general relativistic hydrodynamics to study the origin, evolution, and parametric sensitivity of this instability. We derive the modified conditions of hydrostatic equilibrium for the stars in the curved space of quasi-static orbits. We examine the sensitivity of the instability to the neutron star mass and equation of state. We also estimate limits to the possible interior heating and associated neutrino luminosity that could be generated as the stars gradually compress prior to collapse. We show that the radiative loss in neutrinos from this heating could exceed the power radiated in gravity waves for several hours prior to collapse. The possibility that the radiation neutrinos could produce gamma-ray (or other electromagnetic) burst phenomena is also discussed.

Subject headings: binaries: close — gamma rays: theory — stars: evolution — stars: interiors — stars: neutron

1. INTRODUCTION

In recent numerical studies of the relativistic hydrodynamics of close neutron star binaries in three spatial dimensions (Wilson & Mathews 1995; Wilson, Mathews, & Marronetti 1996, henceforth WMM96), it was noted that as the stars approach coalescence they appear to experience a collapse instability. For an appropriate equation of state (EOS), binary neutron stars might generally become black holes many seconds prior to merger. If correct, this effect could have a significant impact on the anticipated gravity-wave signal from neutron star binaries near coalescence. Such premerger collapse might also be associated with heating, neutrino production, and electromagnetic bursts as the released gravitational energy from collapse is converted into thermal energy of the stars.

Moreover, the numerical evidence that such an instability exists poses a number of new questions such as the sensitivity of the instability to the specific EOS employed, or the intrinsic spin and masses of the stars. One would also like to understand the time history of the collapse and any associated electromagnetic or neutrino emission.

In this paper we present some new three-dimensional calculations that begin to examine these issues. Unfortunately, however, such relativistic hydrodynamic calculations in three spatial dimensions are computationally expensive. A complete systematic study of this instability in three spatial dimensions will be long in coming. In this paper, however, we show that in large part this effect can be replicated in terms of modified one-dimensional spherical relativistic hydrodynamics. We show that the relativistic effects of placing stars in a close binary can be approximated by adding a term involving an average Lorentz-like factor that increases the effective gravitational forces on the stars. The collapse observed in the three-dimensional calculations can be understood in this one-dimensional framework, and one can survey easily the sensitivity of this effect to parameters characterizing the binary and the neutron star EOS.

We can also follow the possible precollapse compression and heating of the neutron star material. This provides a framework in which to model the possible associated neutrino and electromagnetic signals such as gamma-ray bursts. We show that significant heating and neutrino emission is possible as the stars gradually compress before they reach the collapse instability. During the heating epoch the associated neutrino and electromagnetic radiative losses may dominate over the power loss from gravitational radiation.

2. FIELD EQUATIONS

Our method of solving the field equations in three spatial dimensions was discussed in Wilson & Mathews (1995) and WMM96. Here we present a brief review of some features relevant to the present discussion.

We start with the slicing of spacetime into a one-parameter family of hypersurfaces separated by differential displacements in timelike coordinates as defined in the (3+1) formalism (Arnowitt, Deser, & Misner 1962; York 1979).

Utilizing Cartesian x, y, z isotropic coordinates, proper distance is expressed

$$ds^2 = -(\alpha^2 - \beta_i \beta^i)dt^2 + 2\beta_i dx^i dt + \phi^4 \delta_{ij} dx^i dx^j , \quad (1)$$

where the lapse function α describes the differential lapse of proper time between two hypersurfaces. The quantity β_i is the shift vector denoting the shift in spacelike coordinates between hypersurfaces. For an orbiting binary, β_i is dominated by the orbital motion of the system plus a small contribution from frame drag (WMM96). In the frame of one star in the one-dimensional calculations described here, most of the effect of the β_i is transformed away.

The curvature of the three-geometry is described by a position-dependent conformal factor ϕ^4 times a flat-space Kronecker delta. We refer to this gauge choice as the "conformally flat condition" or CFC. For a static system,

the vanishing of the Weyl tensor in three dimensions suggests (cf. Weinberg 1972) that there exists a conformally flat solution to the Einstein equations. One must be careful, however, not to overimpose symmetry conditions (e.g., Cook, Shapiro, & Teukolski 1996). For a dynamic system, one can always impose conformal flatness as an initial condition. There are, however, nonzero time derivatives of the spatial metric and extrinsic curvature that can begin to introduce off-diagonal elements of γ_{ij} as the system evolves. In particular, the imposition of conformal flatness excludes gravity-wave information contained in the transverse traceless components of the metric. However, as discussed below, several recent studies have indicated that this approach is still an excellent approximation when a comparison with exact results can be made.

The implementation of the CFC means that we solve the constraint equations of general relativity at each time as though there were a fixed distribution of matter. We then evolve the hydrodynamic equations to the next time step against this background metric. Thus, at each time slice we can obtain a solution to the relativistic field equations and information on the hydrodynamic evolution. Information on the generation of gravitational radiation can then be obtained from a multipole expansion (Thorne 1980) of the transverse traceless components of the metric.

It is important to appreciate that at each time slice, a numerically valid solution to the field equations is obtained. In this way the strong field properties of the system are included. For this reason, this approach is a significant improvement over a post-Newtonian approach (which is also conformally flat at low order; see the Appendix). The hydrodynamic variables respond to these fields. An approximation we have made herein is the neglect of an explicit coupling of the gravity waves. These, however, contribute negligibly to the metric, stress energy tensor, or hydrodynamic evolution (WMM96). When desired, this coupling can be added via a multipole expansion.

We reduce the solution of the equations for the field variables ϕ and α to simple Poisson-like equations in flat space. We begin with the Hamiltonian constraint equation (York 1979) that reduces to (Evans 1985; WMM96),

$$\nabla^2\phi = -4\pi\rho_1 \, . \tag{2}$$

In the Newtonian limit the source term is dominated by the proper matter density ρ. In the strong field of the orbiting binary, however, ρ must be enhanced by a generalized curved-space Lorentz factor W (cf. eq. [11]). This derives directly from the occurrence of the four-velocity in the stress energy tensor. There are also contributions from the internal energy density $\epsilon\rho$, pressure P, and extrinsic curvature K_{ij}. Thus, we write

$$\rho_1 = \frac{\phi^5}{2}\left[\rho W^2 + \rho\epsilon(\Gamma W^2 - \Gamma + 1) + \frac{1}{16\pi} K_{ij}K^{ij}\right], \tag{3}$$

where Γ is an adiabatic index from the EOS as defined below. Similarly, the lapse function is determined from

$$\nabla^2(\alpha\phi) = 4\pi\rho_2 \, , \tag{4}$$

$$\rho_2 = \frac{\alpha\phi^5}{2} \times \left\{\rho(3W^2 - 2) + \rho\epsilon[3\Gamma(W^2 + 1) - 5] + \frac{7}{16\pi} K_{ij}K^{ij}\right\}. \tag{5}$$

In WMM96 it was shown that the collapse instability can at least in part be traced to the effect of the Lorentz-like factor W on the source density for ϕ and $(\alpha\phi)$. In WMM96 and below it is shown that terms that scale as $(W^2 - 1)$ also enter into the hydrodynamic equations in a way which enhances the gravitational force on each star. In the Appendix we suggest that, even in a post-Newtonian approximation, such terms might cause the effective gravitational potential to be deeper than it would be for static isolated stars.

Regarding the reliability of the CFC as an approach to this problem, we note that a recent study (Cook et al. 1996) has shown that an axially symmetric CFC approximation is quite good when computed physical observables are compared with the exact results for axisymmetric, extremely rapidly rotating, neutron stars. This is the simplest system for which an exact metric begins to differ from a CFC metric.

In another recent application to the nonaxisymmetric case of orbiting binaries Reith & Schäfer (1996) have shown that an expansion using this metric is identical to a post-Newtonian expansion for terms of order $(v/c)^2$. The first deviation appears in terms of order $(v/c)^4$. However, we find that the deviations are small. The expressions in their paper are in terms of a dimensionless parameter $\nu \equiv m_1 m_2/(m_1 + m_2)^2$. It is common in post-Newtonian expansions to compare with a Schwarzschild orbit for which $\nu = 0$. However, for neutron star binaries $\nu = 0.25$ is most appropriate. For equal-mass neutron star binaries $\nu = \frac{1}{4}$ exactly. Even for $m_1/m_2 = 2$ (a relatively large asymmetry for neutron stars) $\nu = 0.22$. For $\nu = 0.25$ the difference between the conformally flat and post-Newtonian $(v/c)^4$ correction for the perihelion advance is about is 4.5%. The $(v/c)^4$ term for the momentum differs by about 2.8%, and the angular momentum term differs by 24.1%. Since $(v/c)^4 \sim 10^{-4}$ for the binaries considered here, these differences in the two-body dynamics are probably insignificant. Note that in the present application we compute an exact instantaneous numerical solution to the Einstein equations using this metric and do not rely upon an expansion that may deviate in individual terms but still provide the correct results. Note also that the principal effect we are investigating here (that due to the $W^2 - 1$ terms) is of order $(v/c)^2$ (see the Appendix), for which the post-Newtonian and conformally flat terms agree exactly. Also, note that the effect described here is a relativistic effect that completely dominates (see below) over the possible stabilizing influence of Newtonian tidal distortion as proposed in Lai (1996). The effect we describe was not considered in that paper.

3. RELATIVISTIC HYDRODYNAMICS

To solve for the fluid motions of the system in curved spacetime it is convenient to use an Eulerian fluid description (Wilson 1979). We begin with the perfect fluid stress-energy tensor, which in covariant form can be written,

$$T_{\mu\nu} = (\rho + \rho\epsilon + P)U_\mu U_\nu + P g_{\mu\nu} \, , \tag{6}$$

where ϵ is the internal energy per gram, P is the pressure, and U_ν is the four-velocity.

By introducing a set of Lorentz contracted state variables it is possible to write the relativistic hydrodynamic equations in a form that is reminiscent of their Newtonian counterparts. The hydrodynamic state variables are the

coordinate baryon mass density

$$D = W\rho \,, \tag{7}$$

the coordinate internal energy density

$$E = W\rho\epsilon \,, \tag{8}$$

the spatial three-velocity

$$V^i = \alpha \frac{U_i}{\phi^4 W} - \beta^i \,, \tag{9}$$

and the coordinate momentum density,

$$S_i = (D + \Gamma E)U_i \,. \tag{10}$$

The Lorentz-like factor W is

$$W = \alpha U^t = \left[1 + \frac{\sum_{i=1}^{3} U_i^2}{\phi^4}\right]^{1/2} , \tag{11}$$

and the EOS index Γ is

$$\Gamma = 1 + \frac{P}{\rho\epsilon} \,. \tag{12}$$

Note that in flat space ($\alpha = \phi = 1$), W reduces to the usual special-relativistic Lorentz factor.

In terms of these state variables, the hydrodynamic equations are as follows:

1. The equation for the conservation of baryon number $(\rho U^\mu)_{;\nu} = 0$ takes the form

$$\frac{\partial D}{\partial t} = -6D \frac{\partial \log \phi}{\partial t} - \frac{1}{\phi^6} \frac{\partial}{\partial x^j} (\phi^6 D V^j) \,. \tag{13}$$

2. The internal energy equation is derived from $T^\nu_{\mu;\mu} = 0$,

$$\frac{\partial E}{\partial t} = -6\Gamma E \frac{\partial \log \phi}{\partial t} - \frac{1}{\phi^6} \frac{\partial}{\partial x^j} (\phi^6 E V^j) - P\left[\frac{\partial W}{\partial t} + \frac{1}{\phi^6} \frac{\partial}{\partial x^j} (\phi^6 W V^j)\right] . \tag{14}$$

3. The spatial components of the momentum conservation condition ($T^\nu_{i;\mu} = 0$) takes the form,

$$\frac{\partial S_i}{\partial t} = -6S_i \frac{\partial \log \phi}{\partial t} - \frac{1}{\phi^6} \frac{\partial}{\partial x^j} (\phi^6 S_i V^j) - \alpha \frac{\partial P}{\partial x^i} + 2\alpha(D + \Gamma E)\left(W - \frac{1}{W}\right) \frac{\partial \log \phi}{\partial x^i} + S_j \frac{\partial \beta^j}{\partial x^i} - W(D + \Gamma E) \frac{\partial \alpha}{\partial x^i} \,, \tag{15}$$

where for the present stability analysis we have set the radiation reaction term (WMM96) to zero.

Regarding the stability of our treatment of numerical relativistic hydrodynamics, we have applied a number of standard tests (e.g., shock tubes, pressureless collapse, etc.) as noted in WMM96. One important test in the present context is that of stable stars in a stable orbit (with no radiation reaction). We have found that for such systems, equilibrium configurations are obtained after a small fraction of an orbit. When the velocity damping is removed there is no discernible change of the stars for several orbit periods. This illustrates an advantage of the shifted grid that we employ. There is essentially no matter motion with respect to the grid once a stable equilibrium has been achieved. Hence, numerical stability can be maintained for a long time.

Another important test is that of a single nonrotating star on the three-dimensional spatial grid. We find that the equilibrium gravitational mass as a function of central density agrees with the spherical hydrostatic Tolman-Oppenheimer-Volkoff equilibrium gravitational mass as a function of central density to within a fraction of a percent. We also find that a dynamical instability ensues once the stellar mass exceeds the maximum hydrostatic mass as expected.

In isotropic coordinates, the condition of hydrostatic equilibrium for the stars ($dS^i/dt = 0$, $V^i = 0$, $\partial \log \phi/\partial t = 0$) can be inferred from equation (15),

$$\frac{\partial P}{\partial x^i} = -(\rho + \rho\epsilon\Gamma)\left[\frac{\partial \log \alpha}{\partial x^i} - \frac{U_j}{\alpha} \frac{\partial \beta^j}{\partial x^i} + \left(\frac{\partial \log \alpha}{\partial x^i} - 2 \frac{\partial \log \phi}{\partial x^i}\right)(W^2 - 1)\right] . \tag{16}$$

Some discussion of the relative magnitude of the terms in equation (16) is useful. The first term with $\partial \log \alpha/\partial x^i$ is the relativistic analog of the Newtonian gravitational force. In the Newtonian limit $\alpha \to 1 - GM/r$. Hence $-\partial \log \alpha/\partial x^i \to GM/r^2$. In equation (16) there are two ways in which the effective gravitational force increases as W exceeds unity. One is that the matter contribution to the source density for α or ϕ is increased by factors of $\sim W^2$ (cf. eqs. [3] and [5]). The more dominant effect is that from the terms in equation (16) that scale as $(W^2 - 1)$. These terms result from the affine connection terms $\Gamma^\mu_{\mu\lambda} T^{\mu\lambda}$ in the covariant differentiation of $T^{\mu\nu}$. These terms have no Newtonian analog but describe a general relativistic increase in the curvature gravitational force as the specific kinetic energy of the system increases. This increase in effective gravity as the stars approach each other can be thought of as a correction to the Newtonian gravity that scales as $(W^2 - 1)$ times the Newtonian gravity. This $(W^2 - 1)$ factor can be thought of as a kind of specific kinetic energy (cf. eq. [11]) from the orbital motion of the binary. The extra $\partial \log \phi/\partial x^i$ term further increases the effect by a factor of 2. This factor comes from $\phi^2 \sim (1/\alpha)$. A further increase of binding arises from the $K^{ij}K_{ij}$ terms in the field sources, but these terms are much smaller than the $W^2 - 1$ contributions.

In our shifted spatial grid, the fluid three velocities V^i are nearly zero. Hence we can use equation (9) to find U_i as a function of β^i. We can also replace β^i in equation (9) with the dominant contribution from orbital motion, $\bar{\beta} \approx \bar{R} \times \bar{\omega}$, where R is the coordinate distance of the stars from the center of mass. Hence, equations (9) and (11) give

$$\langle W^2 \rangle \approx \frac{1}{(1 - \omega^2 R^2 \phi^4/\alpha^2)} \approx \frac{1}{(1 - v^2/c^2)} \,, \tag{17}$$

where $c = \alpha/\phi^2 < 1$ is the coordinate light speed.

In our simulations an effective velocity of $(\omega R/c) \approx 0.25$ is obtained for the last stable orbit of 1.45 $M_\odot$ stars. In the three-dimensional calculations the average $\langle W^2 - 1 \rangle$ typically rises up to $\sim 5\%$ before the orbit becomes dynami-

cally unstable. Thus, we estimate that before orbit instability, the effective hydrostatic gravitational force on the stars is increased by $\sim 10\%$ over that of stationary non-orbiting stars for which $\langle W^2 - 1 \rangle = 0$. This increased gravitational force increases the central densities as the stars approach and can induce collapse.

It is of interest to compare the magnitude of the $(W^2 - 1)$ correction to the Newtonian gravity with the magnitude of the Newtonian tidal energy that would tend to stabilize the star. In Lai (1996) it was estimated that the Newtonian tidal energy should scale as

$$\Delta E_{\rm tidal} \approx -\lambda \frac{GM^2R^5}{r^6}, \tag{18}$$

where for neutron stars $\lambda \approx 0.1$, M is the mass of a star, R is the neutron star radius, and r is the orbital separation. In contrast, the correction to the Newtonian self-gravity from the motion of the stars in a binary is

$$\Delta E_{\rm GR} \approx 2(W^2 - 1) \frac{GM^2}{R}. \tag{19}$$

Taking the ratio of these two contributions, we find

$$\frac{\Delta E_{\rm tidal}}{\Delta E_{\rm GR}} \approx \frac{\lambda}{2(W^2 - 1)} \left(\frac{R}{r}\right)^6 \sim 10^{-4}, \tag{20}$$

where we have used typical values near collapse (cf. Table 1) of $R/r \sim 0.2$ and $(W^2 - 1) \sim 0.05$. Thus, the effect of the increased relativistic gravitational force is expected to dominate over the stabilizing tidal distortion by about 4 orders of magnitude. In a similar analysis, we estimate that even for white dwarfs near merger, this relativistic increase in the gravitational energy exceeds the stabilizing Newtonian tidal energy.

The centrifugal term in equation (16) is dominated by the contribution from orbital motion $U_j(\partial\beta^j/\partial x^i) \approx U_j\omega \sim 10^{-8}$. This term varies little over an individual star, and inside a star this term is small compared to the $\partial \log \alpha/\partial x^i$ term. Hence, this term can be neglected in the discussions of stellar stability. It is important, however, for determining the orbits and gravity-wave frequency (WMM96).

4. EQUIVALENT SPHERICAL MODEL

To better understand the relativistic effects described herein, it is useful to reduce the hydrodynamic equations to an approximate spherical model. Such a model can also be used to make a schematic survey of the sensitivity of collapse to EOS parameters and possible interior heating. From equation (16) we see that the configuration of each star can be described by a modified version of the familiar equation of hydrostatic equilibrium. This is true as long as the contribution of orbital motion to $(W^2 - 1)$ can be treated as a constant factor and the $K_{ij}K^{ij}$ and centrifugal terms can be ignored. Of course, W^2 is not constant over the stars. However, in our three-dimensional calculations it is observed to vary little over the volume of a star.

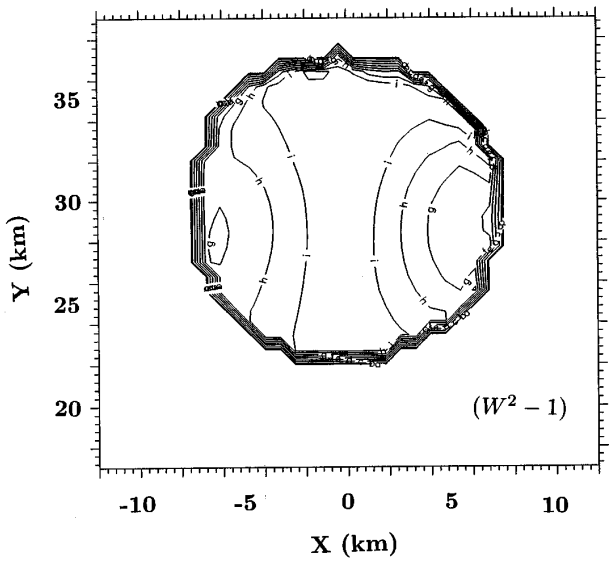

FIG. 1.—Contours of $W^2 - 1$ in the $Z = 0$, X-Y plane from the three-dimensional calculations for $M_G = 1.40$ neutron stars with $J = 2.6 \times 10^{11}$ cm^2. Contour decrease from a maximum of $W^2 - 1 = 0.04$ in steps of 0.005.

Contours of constant $(W^2 - 1)$ from a three-dimensional calculation are shown in Figure 1. From this we deduce that it is not a bad approximation to replace $(W^2 - 1)$ in the source equations and hydrodynamical equations with

$$(W^2 - 1) \approx (W_r^2 - 1 + \langle W_0^2 - 1 \rangle), \tag{21}$$

where W_r is the contribution from radial motion inside a star, and $\langle W_0^2 - 1 \rangle$ is an approximately constant factor that accounts for the influence of orbital motion in the

TABLE 1

PARAMETERS CHARACTERIZING THE ORBIT CALCULATIONS FOR STARS WITH $M_G^0 \approx 1.45\ M_\odot$ AND FOR AN EOS WITH $M_C = 1.70$

	J (10^{11} cm^2)				
PARAMETER	2.2	2.3	2.5	2.6	2.7
M_B ($M_\odot$)	1.598	1.598	1.620	1.620	1.598
M_G ($M_\odot$)	1.416	1.420	1.322	1.317	1.423
f (Hz)	410	310	280	250	267
d_P (km)	39.4	40.6	50.3	50.7	53.0
$\rho_{\rm max}$ (10^{15} g cm^{-3})	2.03	2.70	3.58	2.92	1.93
$\langle W_{3D}^2 - 1 \rangle$	...	...	0.050	0.052	0.043
$\alpha_{\rm min}$	0.440	0.379	0.283	0.288	0.463
$\phi^2_{\rm max}$	1.90	2.05	1.78	2.68	1.84
$\dot{E}$ ($M_\odot$ s^{-1})	0.016	0.0040	0.00048	0.00047	0.0061
Orbit	Unstable	Stable	Stable	Stable	Stable
Stars	Unstable	Unstable	Unstable	Unstable	Stable

NOTE—M_G is the total gravitational mass of the binary divided by 2. Also, f is the gravity-wave frequency, i.e., twice the orbit frequency.

curved spacetime of the binary. The equilibrium and stability of a binary star can then be approximated using a one-dimensional description.

However, since the metric variables α and ϕ depend upon the density distribution, it is not possible to directly compute the hydrostatic equilibrium of the star. Instead, the star must be evolved hydrodynamically (with damping) as $\langle W_0^2 - 1 \rangle$ is increased to obtain the new equilibrium configuration. Hence, we construct a modified spherical hydrodynamic model as follows:

1. For a given distribution of mass and energy, the Poisson equations (2) and (4) for ϕ and α can be integrated directly. The only difference is that the source terms now become:

$$\rho_1 \approx \frac{\phi^5}{2} \{\rho[1 + \epsilon + \epsilon\Gamma(W_r^2 - 1 + \langle W_0^2 - 1 \rangle)]\} , \quad (22)$$

and

$$\rho_2 \approx \frac{\alpha\phi^5}{2} \{3\rho(1 + \epsilon\Gamma)(W_r^2 - 1 + \langle W_0^2 - 1 \rangle) + \rho[1 + \epsilon + 6\epsilon(\Gamma - 1)]\} . \quad (23)$$

2. The hydrodynamic equations become:

$$\frac{\partial D}{\partial t} = -6D \frac{\partial \log \phi}{\partial t} - \frac{1}{\phi^6 r^2} \frac{\partial}{\partial r} (\phi^6 r^2 D V^r) . \quad (24)$$

3. The equation for internal energy conservation becomes:

$$\frac{\partial E}{\partial t} = -6\Gamma E \frac{\partial \log \phi}{\partial t} - \frac{1}{\phi^6 r^2} \frac{\partial}{\partial r} (\phi^6 r^2 E V^r) - P\left[\frac{\partial W_r}{\partial t} + \frac{1}{\phi^6 r^2} \frac{\partial}{\partial r} (\phi^6 W_r r^2 V^r)\right] . \quad (25)$$

4. The momentum equation is:

$$\frac{\partial S_r}{\partial t} = -6S_r \frac{\partial \log \phi}{\partial t} - \frac{1}{\phi^6 r^2} \frac{\partial}{\partial r} (\phi^6 r^2 S_r V^r) - \alpha \frac{\partial P}{\partial r} + 2\alpha(D + \Gamma E)\left[\frac{(W_r^2 - 1 + \langle W_0^2 - 1 \rangle)}{W_r}\right] \frac{\partial \log \phi}{\partial r} - (W_r^2 + \langle W_0^2 - 1 \rangle)(D + \Gamma E) \frac{\partial \alpha}{\partial r} , \quad (26)$$

where we have neglected the centrifugal term as noted above.

The calculations reported here were performed on an Eulerian grid in which the star is resolved into about 100 radial zones.

5. EQUATION OF STATE

A key part of the calculations presented here is the use of a realistic neutron star EOS. The orbital calculations presented in WMM96 used the zero temperature, zero neutrino chemical potential EOS from the supernova numerical model of Wilson & Mayle (1993), Mayle, Tavani, & Wilson (1993). Calculations made with this EOS for a model of supernova 1987A give an explosion energy of 1.5×10^{51} ergs, consistent with observation. Also, the neutrino spectra and time of neutrino emission are in good agreement with the IMB (Bionata et al. 1987) and Kamiokande neutrino detections (Hirata et al. 1987). These models also reproduce the desired abundance distribution of *r*-process heavy elements in the baryon wind from the proto-neutron star (Woosley et al. 1994). The maximum neutron star mass for this EOS as converted to a zero temperature version for our present studies is $M_C = 1.70\ M_\odot$. An important point is that with an EOS that would allow a higher mass neutron star, Wilson & Mayle (1993) were not able to obtain satisfactory results.

In WMM96 only cold equilibrium configurations were computed. However, in the present work we wish to examine the possible heating of the stars as they collapse. Hence, we include finite temperature effects in the EOS. The electron fraction is small for neutron stars $Y_e \ll 1$. Hence, for the heating calculations of interest here, we can relate the temperature to the internal energy by assuming a non-relativistic Fermi gas of neutrons.

We wish to analyze the sensitivity of the collapse instability to the neutron star EOS. To do this we diminish the maximum mass achievable for a given EOS by imposing a maximum value for the index Γ at high density. From this maximum, the adiabatic index asymptotes to 2 at high density to guarantee causality.

We find a maximum neutron star mass of $M_C = 1.55$, 1.64, and 1.70 for $\Gamma_{\max} = 2.297$, 2.346, and 2.470, respectively. This range of masses is consistent with (and even slightly above) the upper range of the observed upper mass limit for neutron stars. Finn (1994) has assigned a lower limit of 1.15–1.35 $M_\odot$ and an upper limit of 1.44–1.50 $M_\odot$ at the 1 σ (68%) confidence level. At the 2 σ (95%) confidence level the upper limit increases to 1.43–1.64 $M_\odot$. In an independent approach, Bethe & Brown (1995) have recently argued from nucleosynthesis constraints that the maximum neutron star mass is 1.56 $M_\odot$. They also point out that if kaon condensation is taken into account the critical mass may only be 1.50 $M_\odot$. If the maximum observed stellar mass were as low as the 1 σ upper limit, i.e., 1.50 $M_\odot$, it could be that almost all neutron star binaries would collapse before coalescence.

With the present state of knowledge of the nuclear EOS at high density, however, it is still possible that the maximum neutron star mass could be significantly greater than 1.70 $M_\odot$. That is, the observed low mass limits may only be an artifact of the way in which neutron stars are formed in Type II supernovae rather than a limit from the EOS. We have made some preliminary studies of stars with $M_G = 1.45\ M_\odot$ for an EOS with $M_C = 1.85\ M_\odot$. We have not observed collapse before the orbit instability is reached. It seems likely that, for a sufficiently stiff EOS, merger will occur as two neutron stars as considered in many Newtonian and post-Newtonian simulations (e.g., Rasio & Shapiro 1992; Zhuge, Centrella, & McMillan 1994; Janka & Ruffert 1996).

6. SUMMARY OF THREE-DIMENSIONAL RESULTS

6.1. *Summary of Previous Results*

In WMM96 orbit calculations were made for two 1.70 $M_\odot$ baryonic mass neutron stars for an EOS for which the gravitational mass in isolation was $M_G = 1.45\ M_\odot$, and the critical neutron star mass was $M_C = 1.70\ M_\odot$. Orbit solu-

TABLE 2

PARAMETERS CHARACTERIZING THE ORBIT CALCULATIONS AT THE FINAL EDIT FOR STARS WITH $M_G^0 = 1.40$ ($M_B = 1.548$) $M_\odot$ IN ISOLATION AND FOR EQUATIONS OF STATE WITH $M_C = 1.70$, 1.64, AND 1.55 $M_\odot$

	J (10^{11} cm^2)						
PARAMETER	2.5	2.6	2.5	2.6	2.5	2.6	2.7
EOS M_C	1.70	1.70	1.64	1.64	1.55	1.55	1.55
M_G ($M_\odot$)	1.300	1.306	1.299	1.306	1.285	1.299	1.310
f (Hz)	270	287	272	251	256	260	233
d_p (km)	62.1	64.8	61.7	65.6	55.3	60.3	68.2
$\rho_{\max}$ (10^{15} g cm^{-3})	1.82	1.79	1.82	1.86	2.95	2.36	1.98
$\langle W_{3D}^2 - 1 \rangle$	0.0384	0.0365	0.0387	0.0354	0.0434	0.0298	0.0339
$\alpha_{\min}$	0.435	0.443	0.426	0.444	0.266	0.396	0.440
$\phi^2_{\max}$	2.05	2.02	2.08	2.02	2.91	2.18	2.02
$\dot{E}$ ($M_\odot$ s^{-1})	0.0016	0.00155	0.00156	0.00141	0.000548	0.00113	0.00112
Orbit	Stable	Stable	Stable	Stable	Stable	Stable	Stable
Stars	Stable	Stable	Stable	Stable	Unstable	Unstable	Stable

tions were sought for three separate values of angular momentum. The neutron stars were taken to be corotating initially, although it was noted that relativistic effects subsequently induce some fluid motion in the stars relative to the corotating frame. In the present study we have not considered the more realistic possibilities of initial neutron star spins or nonequal masses. Such systems contain less symmetry and require a larger computational effort, which we leave for future work.

The first calculation was made with an orbital angular momentum of 2.2×10^{11} cm^2. The stars settled down into what appeared at first as a stable orbit, but later (less than one complete orbit) the stars began to slowly spiral in. The next calculation was made with an angular momentum of 2.3×10^{11} cm^2 for which the orbit appeared stable. However, after about 1 to 2 revolutions the central densities were noticed to be rising. By the end of the calculation the central baryonic densities had continuously risen to about 2.7×10^{15} g cm^{-3} ($\approx$10 times nuclear matter density), which is near the maximum density for a stable neutron star for an EOS with $M_C = 1.70$. It appears that neutron stars of this mass range and the adopted EOS may continue to collapse as long as the released gravitational energy can be dissipated. For this orbit the stars are at a separation distance of $d_p/m = 9.5$, far from merging. By the time the calculation was ended, the minimum α had diminished to 0.379 and ϕ^2 had risen to 2.05 corresponding to a minimum coordinate light speed of 0.18.

A third calculation was made with the angular momentum increased to 2.7×10^{11} cm^2. As can be seen in Table 1 the stars at this separation $d_p/m = 12.4$ seemed both stable and in a stable orbit. However, with only a slight increase in baryonic mass (M_b 1.598 $\rightarrow$ 1.620) a collapse ensues.

6.2. *New Three-dimensional Results*

In the present work, these results are supplemented with additional three-dimensional calculations for initially corotating stars. The new results are obtained with better resolution and an improved treatment of boundary conditions. These calculations have been run several times longer than in WMM96 so that for cases where the instability occurs we have followed the collapse to higher densities and stronger fields.

These new results along with the previous results are summarized in the Tables 1–4. For the star with $M_G \approx 1.45$ $M_\odot$ in isolation, we have added calculations at intermediate orbital angular momenta of 2.5×10^{11} and 2.6×10^{11} cm^2 where we have run for much longer times and further into the collapse. We find that even at 2.6×10^{11} cm^2 the stars collapse while still at a distance of over 50 km apart and with a gravity-wave frequency of only 250 Hz. The collapse instability appears to onset between 2.6 and 2.7×10^{11} cm^2 as $\langle W^2 - 1 \rangle \rightarrow \sim 0.05$ (depending upon the baryon mass).

The rate of energy and angular momentum loss generally increases as the compression proceeds and α becomes small. We note, however, that for unstable stars or orbits, the systems are no longer in quasi-equilibrium orbits. Since the radiated energy and momentum are sensitive functions of separation and ω, the computed values of energy and angular momentum loss become unreliable as an average

TABLE 3

PARAMETERS CHARACTERIZING THE ORBIT CALCULATIONS AT THE FINAL EDIT FOR STARS WITH $M_G^0 = 1.35$ ($M_B = 1.49$) $M_\odot$ IN ISOLATION AND FOR EQUATIONS OF STATE WITH $M_C = 1.70$ $M_\odot$

	J (10^{11} cm^2)					
PARAMETER	1.90	1.95	2.00	2.05	2.10	2.1
M_G ($M_\odot$)	1.225	1.231	1.238	1.243	1.248	1.252
f (Hz)	413	388	365	346	330	312
d_p (km)	46.4	48.4	50.8	52.8	54.8	57.6
$\langle W_{3D}^2 - 1 \rangle$	0.0531	0.0497	0.0459	0.0431	0.0408	0.0388
$\alpha_{\min}$	0.399	0.413	0.428	0.440	0.449	0.457
$\phi^2_{\max}$	2.22	2.16	2.10	2.06	2.02	1.99
$\dot{E}$ ($M_\odot$ s^{-1})	0.0038	0.0034	0.0032	0.0030	0.0029	0.0026
Orbit	Unstable	Stable	Stable	Stable	Stable	Stable
Stars	Unstable	Stable	Stable	Stable	Stable	Stable

TABLE 4

PARAMETERS CHARACTERIZING THE ORBIT CALCULATIONS AT THE FINAL EDIT FOR STARS WITH $M_G^0 = 1.35$ ($M_B = 1.49$) $M_\odot$ IN ISOLATION AND FOR EQUATIONS OF STATE WITH $M_C = 1.55\ M_\odot$

	J (10^{11} cm^2)						
PARAMETER	2.10	2.15	2.20	2.30	2.40	2.50	2.60
M_G ($M_\odot$)	1.238	1.246	1.255	1.262	1.268	1.274	1.279
f (Hz)	270	287	272	251	256	260	233
d_P (km).....	50.6	55.0	57.8	62.5	66.8	70.1	74.4
$\langle W_{3D}^2 - 1\rangle$	0.0476	0.0427	0.0379	0.0350	0.0319	0.0293	0.0272
$\alpha_{\min}$	0.392	0.424	0.452	0.465	0.480	0.493	0.503
$\phi^2_{\max}$	2.23	2.10	2.01	1.96	1.91	1.86	1.83
$\dot{E}$ ($M_\odot$ s^{-1}).....	0.00022	0.0023	0.0022	0.0019	0.0016	0.0013	0.0011
Orbit	Stable	Stable	Stable	Stable	Stable	Stable	Stable
Stars	Unstable	Stable	Stable	Stable	Stable	Stable	Stable

estimate. This is the reason for the lack of monotonicity in the $\dot{E}$ values of Tables 1–4. Eventually, the system approaches two black holes and is no longer well describable in our framework. From the rates of energy and angular momentum loss for these calculations we make a crude estimate (WMM96) that a delay of about 5 s occurs between the collapse instability and the orbit instability for stars with this EOS and $M_G = 1.45\ M_\odot$. This would have interesting consequences on the gravity-wave or electromagnetic signals, as discussed below.

We have also run three-dimensional calculations for stars that would have $M_G = 1.40\ M_\odot$ and $1.35\ M_\odot$ in isolation (Tables 3 and 4). For these systems the EOS was varied as well as the angular momentum. Results from these calculations are summarized in Tables 2–4. We found, as expected, that the $1.40\ M_\odot$ stars are stable for lower angular momenta than the $1.45\ M_\odot$ stars. However, stars of this mass will still collapse for an EOS that is softer. For example, the $1.40\ M_\odot$ star will collapse for $J = 2.6 \times 10^{11}$ cm^2 if the upper mass limit from the EOS is reduced to $1.55\ M_\odot$. We have found that with the $M_C = 1.70\ M_\odot$ EOS it is necessary to reduce the mass to $M_G = 1.35\ M_\odot$ before the stars can survive to final orbit plunge without collapsing first (see Table 3).

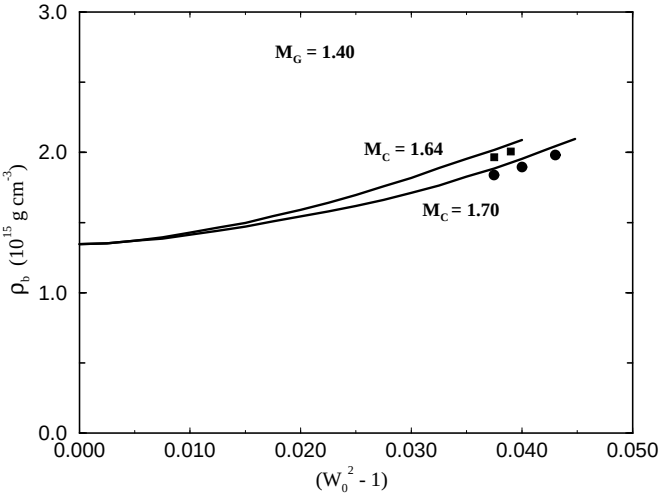

FIG. 2.—Central proper baryon density ρ_c for one-dimensional models (*solid lines*) as a function of $\langle W_0^2 - 1\rangle$ for a star with $M_G = 1.40\ M_\odot$. Lines are drawn for EOSs that give a maximum neutron star mass of $M_C = 1.70\ M_\odot$ and $1.64\ M_\odot$ as labeled. For comparison, the points show numerical results from the three-dimensional calculations at various values of $\langle W_0^2 - 1\rangle$ for the $M_C = 1.70\ M_\odot$ EOS (*squares*) and the $M_C = 1.70\ M_\odot$ EOS (*circles*).

6.3. *Connection to One-dimensional Calculation*

One of the concerns in the three-dimensional calculations of WMM96 was whether the stars and field variables were sufficiently resolved to produce reliable numerical results. In the three-dimensional calculations, the spatial resolution only provided ~10–15 zones in radius across a star. In the one-dimensional calculations, however, one can easily provide many radial zones. We have made a survey of various physical quantities such as the central extrema in α, ϕ, and ρ, as well as the total gravitational mass M_G as a function of the number of radial zones. We have found that there is no significant difference in the field variables, hydrodynamics variables, or gravitational mass as the radial zoning is increased from 15 to 200 zones. Even for only 10 radial zones the error in mass only rises to ~1%. Hence, the zoning in the three-dimensional calculations discussed here and in WMM96 is probably not a significant source of uncertainty.

We wish to explore the reliability of the one-dimensional model as the Lorentz-like factor $\langle W_0^2 - 1\rangle$ is increased. Figure 2 shows the proper central baryon density as a function of $\langle W_0^2 - 1\rangle$. Results are given for two different EOSs; one for which $M_C = 1.64\ M_\odot$; and one with $M_C = 1.70\ M_\odot$. Also shown for comparison are central densities as a function of average values for $(W^2 - 1)$ from three-dimensional calculations. We see that the basic trend of increasing central density with increasing orbital motion is reproduced, although the central density in the one-dimensional calculations is about 2% higher than the three-dimensional calculations for the same average $\langle W_0^2 - 1\rangle$ factor. This suggests that replacing the distribution in W with a mass-weighted average value slightly overestimates the effect. Nevertheless, this approach is sufficiently accurate to apply to the schematic parameter study of interest here.

7. HEATING

In WMM96 the released binding energy was assumed to be deposited only in increased Fermi energy. Any thermal excitation was assumed to be radiated away so that the stars remained cold. However, it is not necessarily true that the input energy above the increasing Fermi energy goes into thermal energy or that it is efficiently radiated away. If this energy were not dissipated, the stars could simply oscillate about the equilibrium rather than collapse. We argue,

however, that it seems most likely that such oscillations would be quickly damped relative to the timescale for inspiraling. Initially, the radial changes will be quite small, and the coupling of radial motion to thermal excitation could occur, for example, via star quakes in analogy with observed pulsar glitches. As the rate of energy release becomes more rapid and the crust melts, we speculate that the coupling of radial modes with the orbital motion, nonradial fluid motion, and tidal forces will lead to a complex excitation of higher modes and shocks that could further heat the star and increase the entropy. Also, the coupling of radial modes with the magnetic fields could damp the oscillations. Eventually, as the stars become hot enough, $T \sim 1$ MeV, neutrino viscosity will serve to damp the radial motion, but this would be late in the evolution.

As these dissipative processes come into play it seems plausible that significant thermal energy could be excited. If the thermal energy is efficiently radiated away, then the stars will remain near zero temperature and the previous calculations are valid. However, it is also possible that the energy may not be radiated away as rapidly as it is released, in which case, the damping will be converted into both increased Fermi energy and thermal energy. An upper limit to the temperature of the star would be that corresponding to no radiation during the compression. In the present work we estimate the possible heating and radiation of the stars as they adjust to the changing orbit $\langle W_0^2 - 1 \rangle$ factor and tidal forces.

If there is sufficient heating, the stars may produce an associated neutrino and/or electromagnetic signal as they compress. Hence, it is of interest to estimate the possible heating of the stars as released binding energy is converted to internal energy.

One can make a simple estimate (Mathews & Wilson 1996) for the heating from the change in gravitational binding energy as the stars compress in the three-dimensional calculations. From Table 1, as J changes by 4×10^{10} cm^2 in the three-dimensional numerical calculations the angular momentum loss rate is $\dot{J} \sim 1$ cm. The time to radiate this change in J is $\Delta J/J \sim 1.33$ s. From the change of binding energy with central density for single stars for a particular EOS, it is possible (Mathews & Wilson 1996) to estimate the energy available for heating of the stars after increasing the Fermi energy. This has an associated change in baryonic mass, hence, it is only an order of magnitude estimate, which we improve upon below.

Nevertheless, this change in binding energy could correspond to a release of as much as 6×10^{52} ergs in thermal energy and a heating rate of 5×10^{52} ergs s^{-1} per star. The corresponding average energy over the stars could be 2×10^{19} ergs g^{-1}. If this energy were injected into a star on the verge of collapse, (central density of 2.42×10^{15} g cm^{-3}) it would heat the core to a temperature $T \approx 45$ MeV (assuming that the core has the heat capacity of a degenerate Fermi gas of neutrons).

This much heating could lead to copious neutrino emission and may provide a framework in which to produce gamma-ray or X-ray bursts. Hence, there is motivation to numerically study this possible heating. We do this in the spherical calculations by imposing an energy-conserving damping term in the equations of motion. This damping relaxes the stars to their new equilibrium. The damped kinetic energy is added as internal energy. By integrating the rate at which kinetic energy is damped into internal and thermal energy, and estimating the fraction that can be subsequently radiated away, we get a measure of the possible heating of the star before collapse.

8. RESULTS

8.1. *Analysis of the Collapse Instability*

With the above one-dimensional approximation to the effects of orbital motion, we can make a systematic study of stellar stability as a function of mass, EOS, and $\langle W_0^2 - 1 \rangle$ factor. First we set $\langle W_0^2 - 1 \rangle = 0$ and run a hydrodynamic calculation at zero temperature with velocity damping until an equilibrium configuration is achieved for a given gravitational mass and EOS. Then we increase $\langle W_0^2 - 1 \rangle$ in small increments and evolve the star hydrodynamically with conservative damping. That is, the damped kinetic energy is added to the Fermi and thermal energy as the calculation proceeds.

For stable stars, we generally observe that the kinetic energy at first rises to a maximum and then damps to zero in the hydrodynamic simulations. For a star that has reached the collapse instability, however, the kinetic energy first rises to a maximum, then falls to a minimum, and then begins to rise again as the collapse ensues. Hence, we define the collapse instability for this systematic study as the point at which the radial kinetic energy begins to increase with time rather than relaxing to zero. We wish to analyze the heating and neutrino emission up to this point. Once the instability is reached, the stars quickly collapse and much of the subsequent heating or neutrino emission becomes lost below the event horizon.

Figures 3–5 show the central value of the lapse α and the released gravitational energy (in units of 10^{53} ergs) E_{53} as $\langle W_0^2 - 1 \rangle$ increases from zero to the point at which dynamical collapse is evident.

Instability in these calculations is also manifest by α decreasing rapidly once it falls below some critical value. In these calculations this instability occurs as $\alpha \rightarrow 0.4$–0.5 depending upon the value of $(W^2 - 1)$, the initial mass, and the EOS. A similar phenomenon has been noted in previous

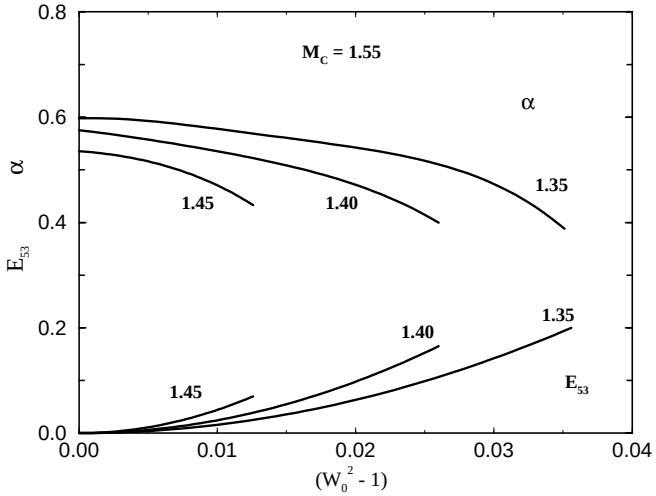

FIG. 3.—Central values of the lapse function α and the released gravitational energy in units of 10^{53} ergs E_{53} as $\langle W_0^2 - 1 \rangle$ increases from zero to the collapse instability point. These calculations use an EOS that gives a maximum neutron star mass of $M_C = 1.55\ M_\odot$. The different curves are labeled by their associated gravitational mass.

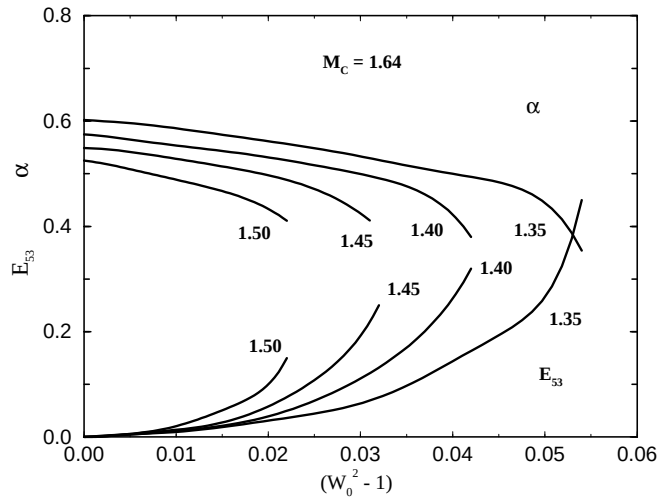

FIG. 4.—Same as Fig. 3, but for an EOS that gives a maximum neutron star mass of $M_C = 1.64\ M_\odot$.

studies of spherical stars in the isotropic gauge. It was noted (Wilson 1979) that once $\alpha < 0.5$ unstable collapse generally ensues, but of course those calculations had no $(W^2 - 1)$ effect. We see the same $\alpha < 0.5$ limit as the mass is increased with $(W^2 - 1) = 0$. The central α in the three-dimensional orbit calculations near collapse is also about 0.4.

The size of the Lorentz factor at instability and the amount of input thermal energy increases with initial gravitational mass M_G and critical mass M_C of the EOS as one would expect. The released energy rises approximately quadratically with $\langle W_0^2 - 1\rangle$. The total energy released up to the instability point increases with decreasing mass and increasing M_C of the EOS.

8.2. *Temperature and Neutrino Luminosity*

The absolute surface neutrino luminosity will depend upon details of the neutrino transport from the interior. It should scale, however, with surface temperature according to a Stefan-Boltzmann law, $L_s \propto T_s^4$, and the total luminosity should scale with the surface radius r and the lapse α_s at the surface, $L_{\rm tot} \propto L_s r^2 \alpha_s^2$.

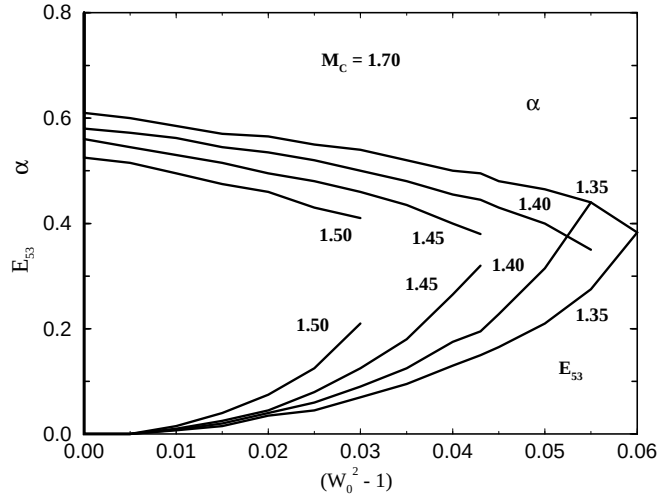

FIG. 5.—Same as Fig. 3, but for an EOS that gives a maximum neutron star mass of $M_C = 1.70\ M_\odot$.

If the luminosity is not as great as the rate at which thermal energy is added to the stars, then central temperatures and the associated neutrino luminosity could be quite high. To estimate the luminosity and temperature as a function of time, consider the Newtonian angular frequency

$$\omega^2 \approx \frac{m}{r^3}\,, \tag{27}$$

and deceleration due to quadrupole radiation (cf. Blanchet et al. 1995),

$$\dot{\omega} = \tfrac{96}{20} m^{5/3} \omega^{11/3}\,. \tag{28}$$

The evolution of ω from earlier times ($t < 0$) up to a value ω_0 can be estimated by integrating equation (28):

$$\omega = \frac{\omega_0}{(1 - (64/5) m^{5/3} \omega_0^{8/3} t)^{3/8}}\,. \tag{29}$$

From equation (27) the time dependence of (m/r) is

$$\frac{m}{r} = \frac{(m\omega_0)^{3/2}}{[1 - (64/5) m^{5/3} \omega_0^{8/3} t]^{1/4}}\,. \tag{30}$$

Since $(W^2 - 1)$ can be thought of as a kind of specific kinetic energy, it should scale as m/r in a stable Keplerian orbit:

$$W^2 - 1 = \frac{\sum U_i^2}{\phi^4} \propto \frac{m}{r}\,, \tag{31}$$

From this we get an approximate time history

$$\langle W_0^2 - 1\rangle = \frac{\bar{W}_{3D}^2 - 1}{[1 - (64/5) m^{5/3} \omega_0^{8/3} t]^{1/4}}\,, \tag{32}$$

where equation (33) is normalized to give the average $\langle W_{3D}^2 - 1\rangle$ factor from the three-dimensional calculation, which has an angular velocity ω_0.

From this relation of $\langle W_0^2 - 1\rangle$ as a function of time it is now possible to construct a possible picture of the luminosity as a function of time. Ideally, one would like to model the detailed thermal neutrino production and transport as released gravitational energy is deposited in the interior. Although we have begun such a calculation, a detailed modeling of the neutrino transport is quite challenging, and it will take some time before a systematic study can be completed. Nevertheless, we can gain qualitative insight into the signal expected from a simple schematic model.

From Figures 3–5 we note that the total input thermal energy grows quadratically with $\langle W_0^2 - 1\rangle$,

$$E_{\rm in} \propto \langle W_0^2 - 1\rangle^2\,. \tag{33}$$

To convert this thermal energy into a luminosity we assume that the neutrino flux through any surface at radius r should scale as

$$F_\nu \propto \left(\frac{r^2 T_0^2}{\rho \kappa_0 T^2}\right) \frac{d(T^4)}{dr} \propto \frac{r^2}{\rho}\, T\, \frac{dT}{dr}\,, \tag{34}$$

where κ_0 is the opacity evaluated at T_0.

The net neutrino flux passing through r is a result of neutrinos diffusing throughout the volume interior to r. To approximate the effective temperature of the flux passing

through r we assume that the thermal energy is deposited uniformly in mass throughout the star. The neutrino flux at any radius r is then taken to be proportional to the mass interior to r,

$$F_\nu \propto m(r) , \tag{35}$$

where

$$m(r) = 4\pi \int_0^r \rho r'^2 \, dr' . \tag{36}$$

Equations (35) and (36) define an effective neutrino temperature profile with radius (cf. Fig. 6)

$$T(r) = A\left[\left(\frac{\int_0^r m(r')dr'}{r'^2}\right) - \left(\frac{\int_0^R m(r')dr'}{r'^2}\right)\right]^{1/2} , \tag{37}$$

where A is a normalization constant. We then solve equations (35)–(38) under the boundary condition that $T = 0$ outside the star, and by equating the total thermal energy at any given time to the integrated thermal internal energy per gram $\epsilon(T)$ for a given temperature and density profile in our the EOS, i.e.,

$$\int_0^R \epsilon(T) 4\pi r^2 \rho \, dr = E_{\rm th} . \tag{38}$$

The radial temperature profile of a 1.40 $M_\odot$ star just as the collapse instability is reached is shown in Figure 6 for the EOSs with $M_C = 1.70$. For this EOS, central temperatures as high as $T \approx 70$ MeV are possible.

The neutrino flux is then calculated using equation (35) with the proper coefficients included. The flux near the surface then gives the luminosity. The luminosity can be used to then define an effective neutrino luminosity temperature,

$$L_\nu = 4\pi R^2 \frac{acT_{\rm eff}^4}{4}\left(\frac{11}{4}\right) . \tag{39}$$

As the stars compress, released gravitational energy can be deposited as internal energy to be radiated away by neutrinos. The rate of accumulated thermal energy is then given by the balance between the rate at which gravitational energy is deposited as thermal energy from the contraction of the stars $\dot{E}_{\rm in}$ and the rate of energy loss L_ν by neutrinos.

We find that the temperature profile as determined above is consistent with a scaling $E_{\rm th} \sim T^2$, where T is evaluated from equation (38) near the surface. This scaling arises because the system can be approximated as a degenerate nucleon gas. Also, from the flux scaling (eq. [35]) we find that $dT/dr \propto T$, so that $L_\nu \sim T^2$. Hence, both $E_{\rm th}$ and L_ν scale with the surface temperature T^2, and we can write

$$L_\nu \propto T^2 \approx kE_{\rm th} . \tag{40}$$

The evolution of the thermal energy can then be written as follows:

$$\dot{E}_{\rm th} = \dot{E}_{\rm in} - kE_{\rm th} . \tag{41}$$

The constant k is evaluated from equation (35) above, and the rate of deposited thermal energy is evaluated from equations (33) and (34).

$$\dot{E}_{\rm in} \approx \frac{dE_{\rm in}}{d\langle W_0^2 - 1\rangle}\frac{d\langle W_0^2 - 1\rangle}{dt} . \tag{42}$$

The analytic solution for the heating of the star then becomes

$$E_{\rm th} \approx e^{-kt}\int \dot{E}_{\rm in} e^{kt'} \, dt' . \tag{43}$$

Figure 7 shows the estimated neutrino luminosity L_ν (in units of 10^{53} ergs s^{-1}), the total accumulated internal energy $E_{\rm th}$ (in units of 10^{53} ergs), and the rate of gravitational energy release $\dot{E}_{\rm in}$ (in units of 10^{53} ergs s^{-1}), for a 1.40 $M_\odot$ star with the $M_C = 1.70$ EOS. These quantities are plotted as a function of time for the last 1.5 s of a star with $M_G = 1.40\ M_\odot$ and an EOS with $M_C = 1.70\ M_\odot$, where the timescale is defined by equation (29).

The total luminosity can become quite significant as the collapse instability is approached. About 4 s before collapse, the neutrino luminosity from each star rises above 10^{51} ergs s^{-1}. The luminosity exceeds 10^{52} ergs s^{-1} about 0.5 s before collapse. The combined neutrino luminosity from the two

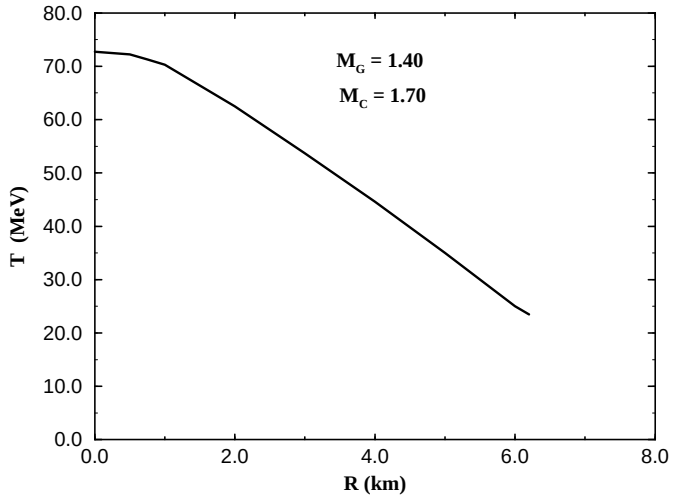

FIG. 6.—Radial temperature profile just as the instability is reached ($\langle W^2 - 1\rangle = 0.055$) of a 1.40 $M_\odot$ star for an EOS that gives a maximum neutron star mass of $M_C = 1.70\ M_\odot$.

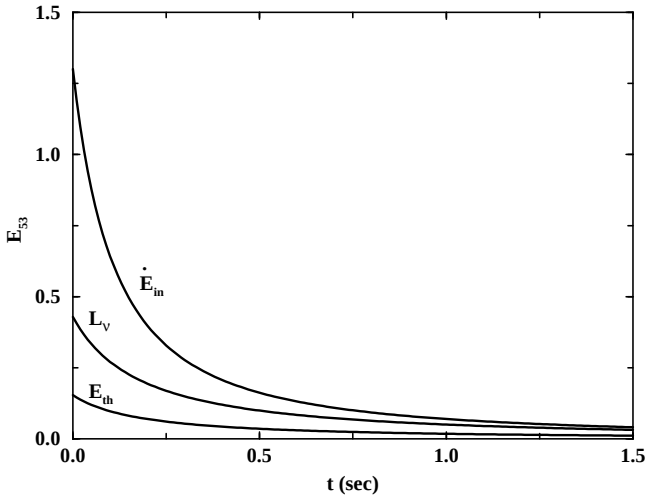

FIG. 7.—Estimated neutrino luminosity L_ν (in units of 10^{53} ergs s^{-1}), the total accumulated internal energy $E_{\rm th}$ (in units of 10^{53} ergs), and the rate of gravitational energy release $\dot{E}_{\rm in}$ (in units of 10^{53} ergs s^{-1}), for a 1.40 $M_\odot$ star with the $M_C = 1.70$ EOS. These quantities are plotted as a function of time for the last 1.5 s of a star with $M_G = 1.40\ M_\odot$ and an EOS with $M_C = 1.70\ M_\odot$.

stars ultimately reaches nearly 10^{53} erg s^{-1} before collapse. This is comparable to the neutrino emission from Type II supernovae, but in this case the emission is from bare neutron stars.

In the quadrupole approximation (Thorne 1980; WMM96), the gravity-wave luminosity $\dot{E}_{\rm GW}$ scales with the square of the $(l+1)$th time derivative of the mass quadrupole moment, $\dot{E}_{\rm GW} \sim Q^2\omega^6 \approx (m/r)^5$. Thus, we write:

$$\dot{E}_{\rm GW} = \frac{\dot{E}^{\rm 3D}_{\rm GW}}{(1-(64/5)m^{5/3}\omega_0^{8/3}t)^{5/4}}\,. \tag{44}$$

From this we estimate that the power (and angular momentum) lost in neutrinos will exceed the energy loss in gravity waves for roughly 3 hr before collapse. This means that the late evolution up to collapse may not be determined by the rate of gravitational radiation but by the hydrodynamics and heat transport of the compressing neutron stars.

If the radiative momentum loss dominates at early times, one may wonder whether it could be observed as an increased slowdown rate in the orbit of a known binary pulsar. We have estimated how much the orbit period of the binary pulsar PSR $-1913+16$ would be affected. Damour & Taylor (1991) have determined that the ratio of the observed orbit period change to the general relativistic prediction is $\dot{P}^{\rm obs}/\dot{P}^{\rm GR} = 1.0081 \pm 0.0022$ (galactic) ± 0.0076 (observational). We estimate that any orbit period change from compressional heating is at least two orders of magnitude below the observational error.

9. CONCLUSION

We have made a survey of the compression, heating, and collapse of neutron stars in close binaries. In particular, we have developed a schematic model to describe when the collapse instability may occur as a function of initial neutron star mass and the EOS. We have also analyzed the possible heating of the neutron star interiors as the stars approach the collapse instability. We find that the stars may obtain quite high thermal energy and neutrino luminosity in the final seconds before collapse. This could have significant implications both for gravity-wave and neutrino astronomy as follows:

9.1. *Implication for Gravity-Wave Detectors*

The analysis here indicates that the radiative neutrino luminosity could exceed the gravity luminosity for hours prior to the collapse instability. If so, this could have a profound influence on the inferred gravity-wave signal. The loss of orbital angular momentum due to neutrinos and electromagnetic radiation will be considerably greater than that of two cold, stable neutron stars. The merger will occur on a shorter timescale, and the gravity-wave signal will be dominated by the dynamics of heating and thermal radiation and not the gravity-wave amplitude up to the point of the instability.

Once the collapse instability is reached, we estimate that the formation of one or two black holes will occur rather abruptly. After collapse, however, the system may not appear simply as two black holes in vacuum. As has been observed in supernova calculations for some time (cf. Mayle & Wilson 1988; Wilson & Mayle 1993) this much neutrino radiation is likely to ablate electron-positron pairs together with baryonic material from the surface of the stars. Baryons ejected in this wind are likely to be present after collapse and may interact with the orbiting objects. To some extent they will provide material to accrete onto the remaining members (neutron star or black holes) of the binary. They may also provide a damping medium that could accelerate the decay of the orbit. Thirdly, this hot wind material may provide a medium in which to anchor the magnetic field lines of the precollapse stars (see Wilson 1975; Ruffini & Wilson 1975; Damour et al. 1978).

We speculate that these effects may serve to accelerate the merger of the two black holes. The interaction of the stars with this medium may affect the dynamics of the black hole inspiral unless the material is ejected with sufficiently high velocity. Clearly, this is an area that warrants further investigation. If our speculation is correct then the gravity-wave signal becomes a probe of the EOS, hydrodynamics, and thermodynamics of the neutron stars as they approach and pass through this collapse instability.

9.2. *Implications for Gamma-Ray Bursts*

The possibility that gamma-ray bursts could be generated by neutrino emission from coalescing neutron stars has been speculated upon for some time. Recently, Janka & Ruffert (1996) have made post-Newtonian hydrodynamics calculations of neutron star mergers and included the neutrino emission therefrom. They find high luminosities, but the timescales are so short ($\sim$ms) that they conclude that it will be difficult to model gamma-ray bursts by neutron star mergers. This short timescale stems from the timescale for mergers. This difficulty is avoided, however, in our model, in which the timescale is set by the gradual compression of the stars. We estimate similar luminosities, but in our model the neutrino luminosity endures for much longer times, thus rendering the possibility of a gamma-ray burst more plausible.

We have shown that significant heating and associated neutrino luminosity is possible in the last seconds before the collapse instability. This poses some interesting possibilities for cosmological models of gamma ray bursts. The thermal emission of neutrinos provides an environment for the generation of an e^+-e^- pair plasma by $\nu\bar{\nu}$ annihilation around the stars. The neutrino emission is occurring in the deepening gravitational well of the two stars. Their interactions will be enhanced by the curved space around the neutron stars. Furthermore, the region between the stars may provide an environment for the buildup of neutrino and matter flux and the production of a pair plasma as desired in some gamma-ray burst scenarios (e.g., Piran & Shemi 1993).

In addition to the collapse-induced neutrino emission itself, the escaping neutrinos are likely to generate a neutrino-heated baryon wind from the stars (Mayle & Wilson 1988; Wilson & Mayle 1993). Unlike in supernovae, the velocity of this wind can be quite high, particularly later in the evolution as the neutrino luminosity grows. This later emission of the high-velocity wind could interact with matter emitted previously, producing shock heating in environments of relatively low optical depth far from the stars. The interactions themselves may contribute to the production of a pair plasma.

As a preliminary test of this scenario we ran a calculation of neutron stars instantly heated such that the surface temperature was $\sim$5 MeV. We then followed the neutrino and matter transport using the numerical supernova model of

Mayle & Wilson (1988). We observed a blow off of the outer layer ($\sim 10^{-5}\ M_{\odot}$) of the neutron star. This material was accelerated to a speed corresponding to a relativistic γ factor of ~ 10. One possibility is that this high-speed matter interacting with magnetic fields and/or interstellar clouds might produce gamma rays.

Finally, we also note that after collapse, the previously ejected material will continue to experience heating either by accretion onto the black holes or by ram pressure from the orbiting stars. Once present, this plasma might become anchored to magnetic field lines around the precollapse stars (Ruffini & Wilson 1975; Damour et al. 1978). The interactions and magnetic recombination of these field lines could also contribute to heating and pair plasma production.

All of these processes may be occurring in the background of the remaining orbiting binary system from times prior to collapse until the final merger to a single black hole. This orbit period may lead to an underlying millisecond substructure in associated burst signals possibly consistent with observations.

Clearly, this is an area that also warrants more investigation. Work along this line is underway to explore such effects as a possible framework in which to model cosmological gamma-ray bursts.

The authors wish to thank P. Marronetti for useful discussions and contributions to this work. Work at the University of Notre Dame was supported in part by DOE Nuclear Theory grant DE-FG02-95ER40934 and by NASA *CGRO* grant NAG 5-3123 and NAG 5-3818. Work was performed in part under the auspices of the U. S. Department of Energy by the Lawrence Livermore National Laboratory under contract W-7405-ENG-48 and NSF grant PHY-9401636.

APPENDIX

POST-NEWTONIAN ANALYSIS OF THE $(W^2 - 1)$ EFFECT

The effect described in this paper stems from a numerical solution to the full Einstein field equations in the approximation that the three metric remains conformally flat. We have interpreted the apparent stellar collapse as the result of a general relativistic increase in the strength of the gravitational acceleration that causes the stars to compresses and heat as the orbit shrinks. At least in part, this increased gravity involves terms that scale with $(W^2 - 1)$. Since $(W^2 - 1)$ can be thought of as a measure of the specific kinetic energy, we interpret this part of the increased relativistic gravity as arising from the increasing mass energy associated with the increasing four-velocity of the binary pair as they approach.

Although we expect that post-Newtonian relativity is a poor approximation in the strong fields near the neutron stars, it is nevertheless instructive to look for this $(W^2 - 1)$ effect in post-Newtonian relativity. One motivation for such an analysis is that the post-Newtonian expansion is an independent approximation to the metric. Hence, it can help to dispel concern as to whether the stellar collapse is somehow an artifact of our metric choice. This exercise can also provide some intuitive insight as to the origin of this phenomenon. In this Appendix, therefore, we outline how a post-Newtonian expansion might exhibit an enhancement of the effective gravitational potential that involves terms scaling as $(W^2 - 1)$.

In the post-Newtonian approximation (see Weinberg 1972) one presumes that it is possible to write the metric as the sum of the Minkowski tensor plus corrections given by an expansion in powers of $v^2 \sim (GM/r)$ in a conformally flat metric. For example, the time-time component of the metric is written

$$g_{tt} = -1 + g_{tt}(2) + g_{tt}(4) \ldots , \tag{A1}$$

where the numbers in parentheses (n) denote terms of order of v^n. From this metric, the corresponding components of the affine connection and Ricci tensor can be similarly expanded. One also decomposes the stress energy tensor into the Newtonian rest mass density plus corrections:

$$T^{tt} = T^{tt}(0) + T^{tt}(2) + T^{tt}(4) \ldots \tag{A2}$$

$$T^{ij} = T^{ij}(2) + T^{ij}(4) \ldots , \tag{A3}$$

where the numbers in parentheses now denote terms of order $(M/r^3)v^n$ and

$$T^{tt}(0) \equiv \rho(1 + \epsilon) . \tag{A4}$$

The remaining $T^{\mu\nu}(n)$ terms then derive from subtracting $T^{tt}(0)$ from the perfect fluid tensor and retaining terms at the appropriate order.

Let us consider only the g_{tt} component of the metric as an indicator of the strength of the gravitational field. For example, the first post-Newtonian correction to the metric, the $g_{tt}(2)$ term, is just

$$\nabla^2 g_{tt}(2) = -8\pi G T^{tt}(0) . \tag{A5}$$

Thus, we have

$$g_{tt}(2) = -2\Phi , \tag{A6}$$

where Φ is just the Newtonian gravitational potential. Velocity-dependent terms enter at the next order. Following Weinberg (1972) we have

$$g_{tt}(4) = -2\Phi^2 - 2\Psi , \tag{A7}$$

where Ψ is a second gravitational potential given by

$$\nabla^2\Psi = \frac{\partial^2\Phi}{\partial t^2} + 4\pi G[T^{tt}(2) + T^{ii}(2)] \, . \tag{A8}$$

To obtain insight into Ψ we first write the appropriate terms from the perfect fluid energy momentum tensor,

$$T^{tt}(2) = \rho(1 + \epsilon)(W^2 - 1 - \Phi) \, , \tag{A9}$$

where the identification of $(W^2 - 1)$ with v^2 is valid at order v^2. The spatial part is just

$$T^{ii}(2) = (W^2 - 1)\rho(1 + \epsilon) + 3P \, . \tag{A10}$$

Thus, the source for the Laplacian of Ψ includes terms that scale as $(W^2 - 1)$ times the mass-energy density plus a smaller contribution from the second-order time derivative of the Newtonian potential:

$$\nabla^2\Psi = \frac{\partial^2\Phi}{\partial t^2} + 4\pi G[2\rho(1 + \epsilon)(W^2 - 1 - \Phi) + 3P] \tag{A11}$$

This suggests how the effective gravitational potential may be deeper for binary stars [where $(W^2 - 1) > 0$] than the static potential of two isolated stars. The total compression effect, however, derives from the covariant derivative of the stress energy tensor as illustrated in eq. (16). One must consider the effective hydrostatic equilibrium of each star, which may involve terms of higher order than first post-Newtonian.

REFERENCES

Arnowitt, R., Deser, S., & Misner, C. W. 1962, in Gravitation, ed. L. Witten (New York: Wiley), 227
Bethe, H. A., & Brown, G. E. 1995, ApJ, 445, L129
Bionata, R. M., et al. 1987, Phys. Rev. Lett., 58, 1494
Blanchet, L., Damour, T., Iyer, B. R., Will, C. M., & Wiseman, A. G. 1995, Phys. Rev. Lett, 74, 351
Cook, G. B., Shapiro, S. L., & Teukolski, S. A. 1996, Phys. Rev. D, 53, 5533.
Damour, T., Hanni, R. S., Ruffini, R., & Wilson, J. R. 1978, Phys. Rev. D, 15, 1518
Damour, T., & Taylor, J. H. 1991, ApJ, 366, 501
Evans, C. R. 1985, Ph.D. thesis, Univ. Texas
Finn, L. S. 1994, Phys. Rev. Lett., 73, 1878
Hirata, K. 1987, Phys. Rev. Lett., 58, 1490
Janka, H. T., & Ruffert, M. 1996, A&A, 307, L33
Lai, D. 1996, Phys. Rev. Lett., 76, 4878
Mathews, G. J. & Wilson, J. R. 1996, in AIP Conf. Proc. 384, Gamma-Ray Bursts: 3rd Huntsville Symp., ed. C. Kouveliotou, M. Briggs, & G. J. Fishman (New York: AIP), 768–771
Mayle, R. W., Tavani, M., & Wilson, J. R. 1993, ApJ, 418, 398
Mayle, R. W., & Wilson, J. R. 1988, ApJ, 334, 909
Piran, T., & Shemi, A. 1993, ApJ, 403, L67
Rasio, F. A., & Shapiro, S. L. 1992, ApJ, 401, 226
Reith, R., & Schäfer, G. 1996, preprint
Ruffini, R., & Wilson, J. R. 1975, Phys. Rev. D, 12, 2959
Thorne, K. S. 1980, Rev. Mod. Phys., 52, 299
Weinberg, S. 1972, Gravitation and Cosmology (Wiley: New York)
Wilson, J. R. 1975, Ann. N. Y. Acad. Sci., 262, 123
———. 1979, in Sources of Gravitational Radiation, ed. L. Smarr (Cambridge: Cambridge Univ. Press), 423
Wilson, J. R., & Mathews, G. J. 1995, Phys. Rev. Lett., 75, 4161
Wilson, J. R., Mathews, G. J., & Marronetti, P. 1996, Phys. Rev. D, 54, 1317 (WMM96)
Wilson, J. R., & Mayle, R. W. 1993, Phys. Rep., 227, 97
Woosley, S. E., et al. 1994, ApJ, 433, 229
York, J. W., Jr. 1979, in Sources of Gravitational Radiation, ed. L. Smarr (Cambridge: Cambridge Univ. Press) p. 83
Zhuge, X., Centrella, J. M., & McMillan, S. L. W. 1994, Phys. Rev. D, 50, 6247